Nanoscale Advances

ROYAL SOCIETY OF CHEMISTRY

PAPER

View Article Online
View Journal

Cite this: DOI: 10.1039/d5na01038a

Unravelling the interplay between structures, self-assembly patterns, AIEE and chiroptical properties of NDI-bis-cholesteryl systems

Gargee Roy, Aakash Ravikant Likhar and Deepak Asthana *

Naphthalene diimides (NDIs) offer exquisite optical and electronic properties and find a broad range of applications in various chemical and biomedical fields. However, due to their flat structure, at higher concentrations, the emission from NDIs gets severely quenched. The restoration of luminescence in such an interesting class of molecules has been widely explored through the tuning of their optical properties *via* synthetic modification, supramolecular self-assembly and aggregation induced emission (AIE) techniques. Here, we aim at highlighting the role of the spacer group in the tuning of the chiroptical properties of NDIs through a self-assembly approach, using a bis-cholesteryl diimide system. Three NDI-bis-cholesteryl systems have been prepared and their self-assembled structures, optical and chiral properties in monomeric and aggregated states have been studied. Microscopic investigations reveal almost identical morphology in aggregates, however, quite different aggregation behaviour and chiroptical properties in the ground and excited states are observed. Circular dichroism (CD) studies revealed an interesting medium controlled enhancement and reversal of chiral properties in the self-assembled structures.

Received 8th November 2025
Accepted 28th December 2025

DOI: 10.1039/d5na01038a

rsc.li/nanoscale-advances

Introduction

The distinctive use of non-covalent interactions leading to the formation of ordered and complex aggregates is the foundation for an eminent domain of chemistry referred to as supramolecular chemistry. Supramolecular self-assembly is an instinctive process that is usually triggered by solvent polarity and is guided by relatively weak intermolecular forces, namely hydrogen bonding, van der Waals forces, dipole–dipole interactions, and π–π stacking interactions. Small structural, or sometimes conformational differences induced by an external stimulus, may steer the intermolecular attractive forces in different directions and result in morphological and chiral transformations.[1–8] Self-assembled supramolecular structures from various functional molecular materials have been noted to possess improved and exceptional properties that are viable for device fabrication.[9–15]

Among various other organic scaffolds, naphthalene diimides (NDIs) are perhaps the most extensively applied building blocks.[16,17] The possibility of functionalization at both bay and core positions, allows formation of various NDI-systems that find diverse applications in materials, and display interesting biological activities.[18–21] NDIs have been exploited predominantly in the field of organic electronics, sensing, light harvesting, opto-electronics, and other light-emitting devices.[22–32] NDIs can often be modified to produce well-organized nanoarchitectures thereby providing a control over desired photophysical properties.[16,33–35] This property of NDIs has been utilized to design various systems that exhibit aggregation induced enhancement of emission (AIEE), a much desired property that avoids concentration-caused quenching.[36–40] Besides AIEE, another interesting property of fluorescent systems is circularly polarised luminescence (CPL), which requires a chiral environment.[41] Naphthalene imides and naphthalene diimides have been proven to be noticeably useful in designing highly efficient organic CPL materials.[42–44]

It is well understood that NDIs tend to self-assemble *via* π–π stacking interactions, and the mode of supramolecular network formation, *e.g.* J- or H- type aggregates, plays a crucial role in the observed optical or chiroptical properties of NDI systems.[45–47] Therefore, gaining a deep understanding about the structural factors that may alter the optical properties in the bulk becomes ineluctable. In the past, various studies have been dedicated to finding the correlation between the molecular structure of NDI derivatives and the resultant self-assembled nanostructures.[40,48–52] Having information about possible molecular packing modes would help in attaining control over the long-range order in self-assembled nanostructures.

Forming diimides of naphthalenetetracarboxylic dianhydride (NTCDA) are not greatly explored for functional applications; instead, modification at the core positions has been used as a major strategy to modulate the optical and electronic properties of NDIs.[17,53,54] However, core substitution

Department of Chemistry, Ashoka University, Sonipat, Haryana, 131029, India. E-mail: deepak.asthana@ashoka.edu.in

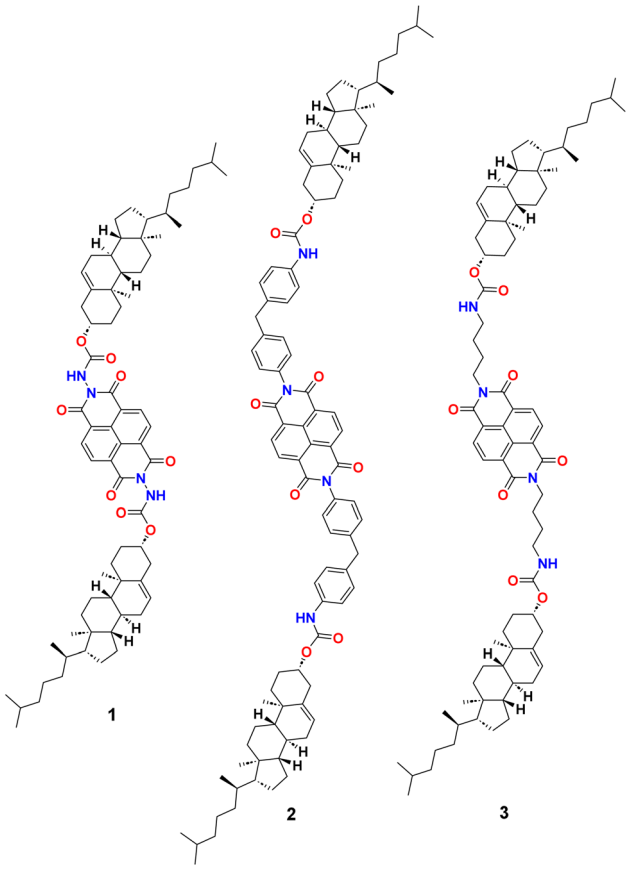

Scheme 1 Chemical structures of NDI derivatives (1, 2 and 3).

is a tedious and complicated process involving rigorous multi-step synthesis. We focused on functionalization of NTCDA through imide formation using cholesteryl units. Due to its benign nature, cholesteryl has been widely used as a hydrophobic unit in NDIs and various systems, where small structural variations have been utilized to tune the supramolecular and photophysical properties of the molecules.[48,55–57] In polar environments and aqueous media the cholesteryl unit incites the aggregation and facilitates a chiral bias to the molecular assembly owing to the availability of multiple stereocentres.[58,59]

Herein, we have prepared three NDI systems (**1–3**) having two cholesteryl units at imide positions connected through different types of spacer groups (Scheme 1). The spacer groups are chosen to provide tuneability in molecular packing. Molecules **1** and **2** have rigid linkers, whereas, molecule **3** has four CH_2-group long alkyl spacers that provide sufficient flexibility to the cholesteryl units. Molecule **3** having a flexible linker can have lots of adjustments during the molecular self-assembly to attain the most stable molecular packing scheme.

Results and discussion

Synthesis and characterization

All the compounds were synthesized by following standard methods reported elsewhere. For preparation of compounds **1** and **2**, first cholesteryl chloroformate was reacted with hydrazine or 4,4′-methylenedianiline to give mono-cholesterylcarboxylated intermediate products, which were then refluxed with NTCDA in dimethyl formamide (DMF) to give compounds **1** and **2**. In the case of compound **3**, first an excess amount of 1,4-diaminobutane was reacted with di-*tert*-butyl dicarbonate (Boc anhydride) to obtain *tert*-butyl (4-aminobutyl) carbamate, which was then refluxed with NTCDA in the presence of DMF. The obtained diimide was treated with trifluoroacetic acid (TFA) to deprotect the amino group and then was reacted with cholesteryl chloroformate in dichloromethane in the presence of triethylamine to produce compound **3**. All the compounds were then characterized by various analytical methods such as ^{1}H and ^{13}C NMR, mass spectrometry (MALDI) and FT-IR. The detailed synthetic procedure and characterization data can be found in the supplementary information (SI).

Photophysical studies

Compounds **1–3** are designed to undergo a self-assembly process in polar solvents. Molecular aggregation may lead to the formation of either J- or H-type of assembly which can be investigated through optical measurements. In some cases, the solvent may function as a trigger to switch the aggregate type. We carried out UV-Vis absorption studies to explore the role of solvents in the aggregation behaviour of compounds **1**, **2** and **3**. As expected, all three compounds show high solubility in less polar solvents like chloroform, dichloromethane, *etc.* For our studies we chose tetrahydrofuran (THF) as the solvent in which all compounds remain soluble at quite high concentration and it allows investigations to be performed in highly polar solvent mixtures such as THF/H_2O. UV-Vis absorption spectra of 20 μM solution of compounds **1–3** in THF showed characteristic absorption bands at around 340 nm, 355 nm and 375 nm corresponding to S_0–S_1 transitions and fine vibronic π–π* transitions (Fig. 1).[60,61] Changing the solvent from polar THF to dichloromethane (DCM) affects the absorption spectra in a non-uniform way (Fig. 1d). In the case of compounds **1** and **3**, we

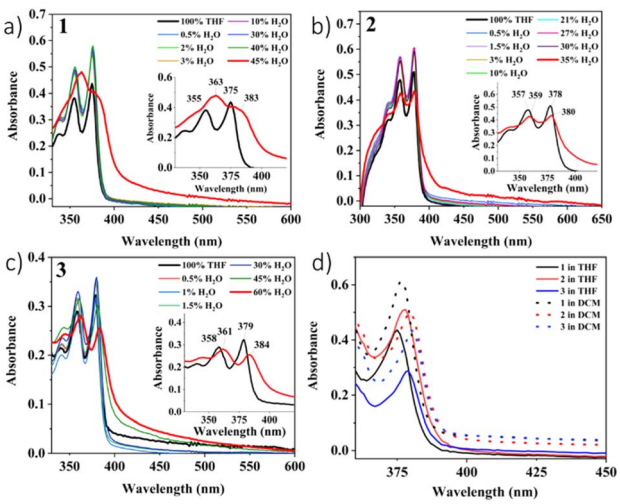

Fig. 1 UV-Vis absorption spectra of compounds **1–3** [20 μM] in the THF/H_2O solvent mixture (a–c) and in THF & DCM (d).

observed a slight red shift and significant increase in absorbance, whereas, for compound **2**, there was a slight decrease in absorbance.

We noticed that addition of water to THF solution causes the solution to turn turbid due to the appearance of aggregated structures. We measured the absorption spectra of compounds **1–3** in a THF/H_2O mixture and varied the water proportion to gain information about tuning of optical properties *via* self-assembly formation (SI Fig. S1). Initially, as the proportion of water is increased, the polarity increase in the solvent causes an increase in the absorbance with little shift in the absorption bands (Fig. 1a–c). However, after reaching a certain percentage of water in the mixture, further increase results in a quick drop in absorbance, and this value (water percentage) differs for each compound. The observed slight red shift in the absorption band could be attributed to the formation of J-type aggregates leading to offset π-stacking interactions. For compound **1**, when water reaches 45% in the THF/H_2O mixture, a bathochromic shift of around 8 nm is observed. A similar trend is observed for compound **3**, however, the red shift is smaller (5 nm) and the percentage of water required in the THF/H_2O mixture to reach the transition point is much larger (60%). Surprisingly, in compound **2** the sudden decrease in absorbance occurred at 35% water and showed no shift in the absorption wavelength. At higher water percentages large aggregates started forming and the sample lost its transparency.

To gain deeper insight into polarity *vs.* aggregation induced changes, we further checked the absorption spectra of compound **3** in hexane and hexane/EtOH mixtures (Fig. S1d). Increasing the EtOH percentage in the hexane/EtOH mixture resulted in continuous increase in absorbance with nearly no change in the absorption band position. Changing ethanol from 40 to 60% in the mixture showed a decrease in absorbance, like the one seen in THF/H_2O. Although the absorbance follows a similar trend in both THF/H_2O and hexane/EtOH mixtures, no red shift in the latter case negates the formation of J-type aggregates, which are observed in the former.

To gain information about required water content in the solvent mixture to trigger self-assembly, we performed a concentration dependent UV-Vis absorption study for molecule **1**. Absorption spectra of a 2 μM solution of **1** required 60% water to reflect the same bathochromic shift that is observed for a 20 μM solution in 45% water (Fig. S1e). When a higher concentration sample is used [100 μM], the requirement of water proportion dropped to 40%.

We then started evaluating the emission properties of these compounds. When excited at 370 nm, THF solutions of compounds **1–3** show fluorescence peaks centred around 421, 421 and 407 nm, respectively. Emission spectra of **1–3** in DCM revealed that the solvent polarity has a significant influence on the fluorescence intensity of these compounds (Fig. 2d). As can be seen, changing the solvent from THF to DCM results in a decrease in the fluorescence intensity of compounds **1** and **2**. In contrast, compound **3** exhibited higher fluorescence intensity in DCM. As we have already seen from the absorption studies of compounds **1–3** the presence of water showed modulation of optical properties by triggering the self-assembly

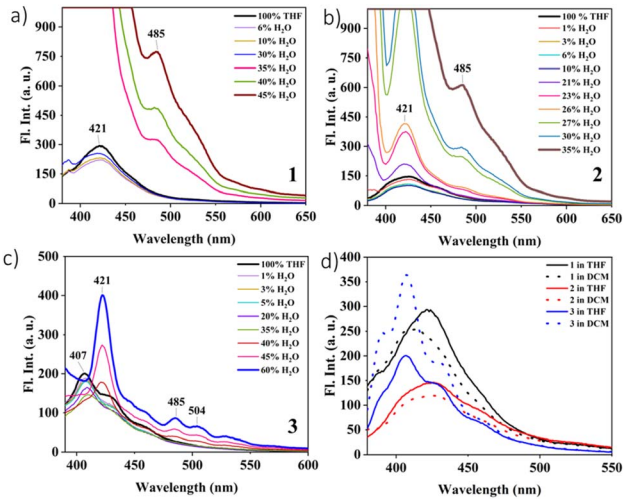

Fig. 2 Emission spectra (λ_{exc} = 370 nm) of **1–3** [100 μM] in the THF/H_2O solvent mixture (a–c) and in THF and DCM (d).

process. We performed the fluorescence measurements in THF/H_2O mixtures to understand the influence of aggregation behaviour on emission properties.

Fluorescence spectroscopy of compounds **1–3** [100 μM] in varying THF/H_2O solvent mixtures revealed a very interesting pattern in the fluorescence intensities and confirmed the AIEE phenomenon in all three compounds (Fig. 2a–c). When a small amount of water is introduced in THF, quenching of the fluorescence intensity is observed, which is expected for water.[62] For compound **1**, addition of merely 6% water causes a nearly 19% drop in the fluorescence intensity (SI Fig. S3). This quenching is overcome by further addition of water. Due to the strong hydrophobic nature of the compound, increasing the water proportion in the mixture initiates the self-assembly process. In aggregated form, the AIEE becomes strongly favoured, and the fluorescence intensity starts to increase. Up to 30% water in the THF/H_2O solvent mixture, the fluorescence intensity remains lower than the fluorescence intensity observed in only THF; however, a drastic increase in the intensity takes place when water was increased to 35%. At this level, the fluorescence spectrum gets saturated.

A similar trend in the fluorescence intensity change with respect to the percentage of water in THF/H_2O is also observed for compounds **2** and **3** (Fig. 2b and c). For compound **2**, the initial fluorescence quenching due to added water is fully restored at around 20% water content. Further increase in water increases the fluorescence intensity. The sudden increase in intensity that is observed for **1** at 35% occurs in the range of 25% to 27% for **2**. This implies stronger AIEE behaviour in compound **2**. The emission spectrum for compound **3** could not be measured under identical conditions, as the fluorescence intensity at 100 μM and a slit width of 20 mm (conditions for measurement of compounds **1** & **2**) was too high to be measured. Therefore, for compound **3**, we kept the concentration the same (100 μM) but decreased the slit width to 10 mm.

For compound **3**, the initial quenching due to addition of water was more severe than that of compounds **1** and **2** (Fig. 2c),

where fluorescence intensity kept on decreasing until a 35% water ratio. A slight red shift in the emission wavelength was also noticed. It required 40% water in the mixture to exhibit AIEE and finally 45% water was enough to make the intensity higher than in THF alone. An approximately 14 nm red shift in the emission wavelength was also obvious to observe. The observed difference in their fluorescence behaviour and AIEE properties might be attributed to the difference in their structures that makes compound **3** more flexible allowing large adjustments in its supramolecular assembly than the compound **1** or **2**.

Having observed the strong aggregation behaviour of compounds **1–3**, and considering the fact that the cholesteryl unit usually favours supramolecular gel formation, we investigated the gelation ability of the synthesized compounds. To our surprise, all our attempts to find a gelation condition failed, except one, in which we could get an opaque gel (2 wt%) of compound **3** in the hexane/EtOH (1 : 6) mixture.

To gain more information about the AIEE properties, we measured the absolute Photoluminescence Quantum Yield (PLQY) of **1–3** in both dilute solutions and aggregated states. The PLQY values for **1**, **2** and **3** in THF were found to be 6.2%, 4.4% and 14.0% respectively. The PLQY values increase to 8.5%, 4.6% and 17.1% when measured in a THF/H_2O mixture having 45% H_2O.

In general, NDI-based compounds bearing no substituents at core positions exhibit either no or very poor solid-state photoluminescence (SSPL) properties, except for a few systems.[44,48,49,63,64] As for any real life applications in the form of devices, it is desirable to have SSPL, we measured the emission spectra using powdered samples of **1**, **2** and **3** (Fig. 3a). The spectra showed broad emission bands centred around at 417 nm, 421 nm and 454 nm, respectively. The observed SSPL peaks for compounds **1** and **2** are in close resemblance to the emission profile found in solution. However, for compound **3**, in the SSPL spectrum, a bathochromic shift of about 30 nm with respect to solution emission, is observed. Significant contribution from excimer emission might be the reason behind broadening of the solid-state emission spectrum of **3**.

We further examined the powder X-ray diffraction (PXRD) patterns of compounds **1–3**. Among the three prepared bis-cholesteryl NDI derivatives, compound **1** showed more defined peaks, indicating better crystallinity in the sample. Due to poor crystallinity, the peaks around $2\theta = 25$–$28°$, which help in predicting π–π stacking modes, are not well defined. Lack of those peaks in PXRD hints towards formation of J-type aggregates,[65] which aligns with the UV-Vis measurements.

In order to further delve into the understanding of AIEE, time-resolved photoluminescence (TRPL) measurements were done for all three compounds in both the solution and aggregated states using different solvent combinations of THF/H_2O and hexane/EtOH (Fig. 4a–c). The excited-state fluorescence lifetime decay profiles ($\lambda_{ex} = 370$ nm) exhibited a bi-exponential decay pattern. Fluorescence lifetime in THF is found to be 1.25 ns, 1.82 ns and 1.54 ns for compounds **1–3**, respectively. Adding 20% water to THF resulted in an increase in lifetimes for all three compounds. Increasing the water content further in the mixture, caused a decrease in lifetime. This shows faster decay in the aggregated state. We further checked the excited state lifetime for compound **3** in hexane/EtOH mixtures, where it showed gelation properties, and observed a similar trend. Lifetime in hexane is found to be 1.23 ns, which decreased to 1.13 ns and finally to 1.04 ns in 20% and 45% hexane/EtOH mixtures, respectively.

As compounds **1–3** are designed to have different linkages between the naphthalene moiety and cholesteryl groups, we got interested in analysing the formed nanostructures to understand the impact of these structural differences on their self-assembled structures. Field emission scanning electron microscope (FE-SEM) images obtained from the sample prepared from a [100 μM] solution of **1** and **2** in a 10% H_2O/THF mixture revealed formation of cylindrical structures that are several micrometres in length (Fig. 5). A closer look at those cylindrical rod-like structures showed that they have a mesh-like morphology. It is visible from the higher resolution images that self-assembled molecular aggregates further form an intertwined network of nanostructures, giving rod-like appearances. In the case of compound **3**, similar molecular aggregates are formed, but they fail to attain any particular shape in the bulk.

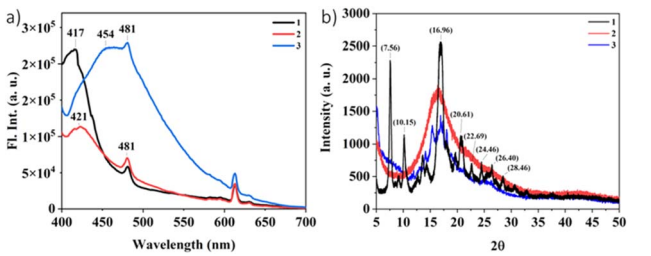

Fig. 3 (a) SSPL spectra of powdered samples and (b) PXRD spectra of compounds **1–3**.

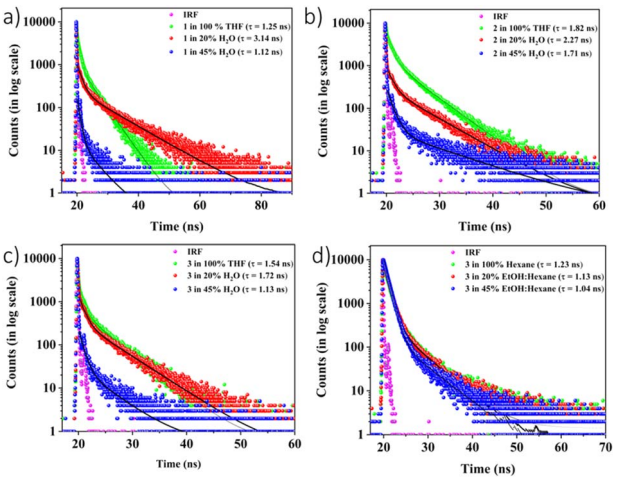

Fig. 4 Plots showing fluorescence lifetime decay curves ($\lambda_{ex} = 370$ nm) and corresponding fit (solid black line) for compounds **1–3** [20 μM] in THF/H_2O (a–c) and for compound **3** in hexane/EtOH (d).

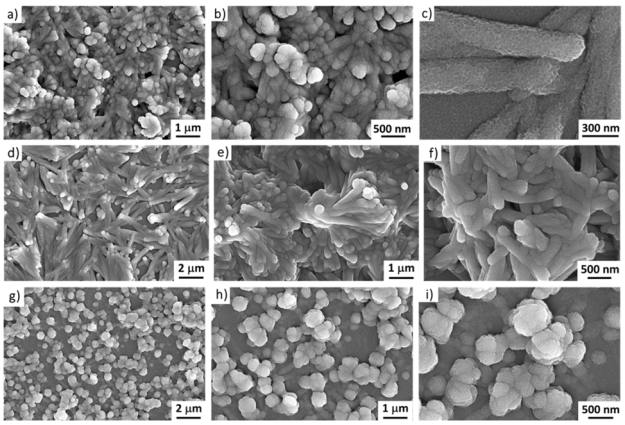

Fig. 5 FE-SEM images obtained from 10% THF/H_2O samples of **1** (a–c), **2** (d–f), and **3** (g–i).

Circular dichroism (CD) and CPL measurements

Inclusion of cholesteryl units in the molecular design introduces chirality in the system. Chiral chromophores are of special interest for their chiroptical properties desirable for chiral sensing, switches, circularly polarized luminescence, *etc.*[13,66,67] As a Circular Dichroism (CD) spectrum provides an insight into the ground electronic state of a chiral compound, we measured the CD spectra of the synthesized NDI-bis cholesteryl derivatives (**1–3**). To understand the effect of structure variation on the overall chiral properties of these compounds, we performed measurements using aggregated samples obtained from [50 μM] solution in the 50% THF/H_2O solvent mixture (Fig. 6a). Under these conditions, compound **1** showed strong CD absorption bands around 343 nm and 382 nm corresponding to the absorption bands of the NDI moiety. The NDI absorption bands for compounds **2** and **3** were there but weak in intensity. We further calculated the g_{abs} values for compounds **1–3**. For the absorption peak at 250 nm, the g_{abs} shows a value of −0.028, +0.001, and −0.002, respectively. To clarify this, we measured the CD spectra of compounds **2** and **3** in higher concentration [100 μM] samples prepared in 50% THF/H_2O (Fig. 6b). Interestingly, the sign of CD bands which is +ve for compound **2**, changes to −ve for compound **3**. This type of behaviour is usually observed in the case of enantiomers where if one stereoisomer shows a +ve signal, then the other stereoisomer shows a −ve signal.

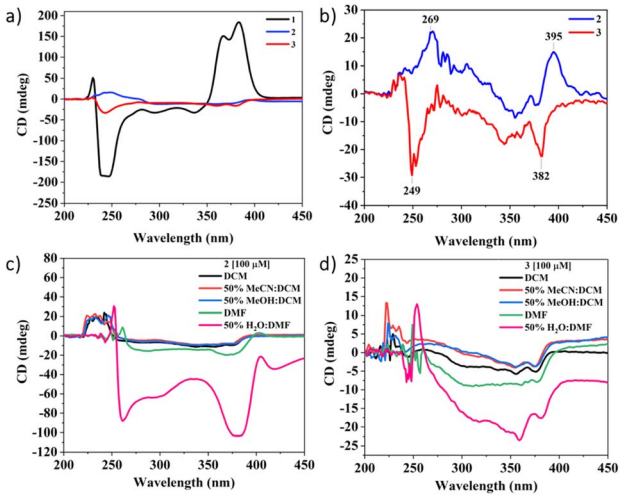

Fig. 6 Room temperature CD spectra of compounds in 50% THF/H_2O: (a) **1–3** [50 μM] and (b) **2** and **3** [100 μM]. Plots (c) and (d) show CD spectra of compounds **2** and **3** [100 μM] in DCM, 50% DCM/MeCN, 50% DCM/MeOH, DMF, and 50% DMF/H_2O.

To correlate the observations made during investigation of self-assembly and its impact on the emission spectra of compounds **1–3**, we performed CD measurements in THF and THF/H_2O mixtures. For compound **1** [50 μM], we found that CD spectra remained very weak in both THF and 20% H_2O/THF solvents (SI Fig. S7a). However, when the water proportion is doubled, making it 40% in the H_2O/THF mixture, the intensity of CD spectra increases dramatically between 325 nm and 425 nm, and then gets saturated. CD spectra of compounds **2** and **3** [100 μM], with varying amounts of water in THF/H_2O did show an increase in the signal intensity, but the difference was not as remarkable as that seen with compound **1** (SI Fig. S7a).

To understand the role of polarity of the solvent medium in the overall chiral behaviour in the bulk, we further performed CD measurements in solvents with varying polarities. CD spectra of compounds **1–3** in DCM, 50% DCM/MeCN, 50% DCM/MeOH, DMF and 50% DMF/H_2O were recorded. In the case of compound **1** [50 μM], the CD spectrum initially showed a −ve CD signal centred around 350 nm, which became less −ve when the solvent was changed to DMF, 50% DCM/MeCN or DCM/MeOH. Upon changing the solvent to DMF, the CD signal looked opposite to the one observed in DCM, indicating a complete inversion of helicity (SI Fig. S7d). This is in agreement with the CD spectrum observed in 50% THF/H_2O where the CD signal corresponding to the NDI absorption band is +ve (Fig. 6a).

Similar CD measurements performed for compounds **2** and **3** [100 μM] revealed very interesting results (Fig. 6c and d). For compound **2**, while there was no significant change in the CD signal intensity upon changing the solvent from DCM to 50% DCM/MeCN or DCM/MeOH, an increase in intensity was observed for DMF. However, a drastic increase in signal intensity took place when the solvent was changed to 50% DMF/H_2O (Fig. 6c). CD signal signs are opposite to the one observed in 50% THF/H_2O (Fig. 6b). Therefore, a reversal in helicity is observed for compound **2** as well. Compound **3** measured under similar conditions showed the expected increase in signal intensity, but no reversal of CD signal sign was observed (Fig. 6d). These results prove the role of solvent medium in deciding the helicity of self-assembled nanostructures in the bulk.

Seeing encouraging CD data and impressive AIEE behaviour, we got interested in exploring CPL activity of these compounds in the solid state and under various solution conditions. Using a JASCO CPL-300 CPL spectrometer, we performed measurements for compounds **1** and **3** in a 1 : 1 THF/H_2O mixture, and compound **2** in a 1 : 1 DMF/H_2O mixture. Excitation at 350 nm failed to provide any detectable CPL signal for compounds **1–3**.

We further investigated the solid-state CPL spectrum for compound **1** in the pellet form; however, this too could not exhibit any CPL activity. Therefore, although compounds **1–3** show interesting CD and AIEE properties, they lack the ability to emit circularly polarized light. Further design modification would be required to achieve this.

Conclusions

To summarize, here we have prepared three symmetric NDI derivatives bearing two chiral units in the form of cholesteryl groups at imide positions. The spacer, that connects the cholesteryl group with the nitrogen atom of the NDI, is varied. In compounds **1** and **2** the spacer provides a rigid linkage in which the cholesteryl groups stay tightly fixed in a specified orientation. However, in compound **3**, in which four $-CH_2$ groups are used, the linkage remains very flexible and allows a lot of freedom to the cholesteryl groups. This structural difference affects the mode of packing in molecular self-assembly. Using water as a trigger to initiate the self-assembly process in THF/water mixtures, we have explored the impact of the small structural variation on the absorption, emission, and chiral properties of these systems. Interestingly, all these compounds show AIEE properties and we could also obtain the minimum amount of water in THF to trigger AIEE behaviour, *e.g.* for compound **1** [100 μM], changing the water proportion from 30% to 35% results in a sudden and steep rise in fluorescence intensity. Additionally, although all three compounds carry the same chiral unit, cholesteryl groups, compound **1** exhibits the strongest CD signals under identical measurement conditions. Another interesting feature that we observed is that compounds **2** and **3** display opposite chirality in the same solvent system. We also demonstrated how THF/H_2O and DMF/H_2O can be used to change the helicity in the self-assembled nanostructures. This information may provide vital suggestions for designing new chiral fluorophores for AIEE and CPL systems.

Author contributions

GR synthesized the reported molecules and collected the data. GR and ARL analysed the data. DA supervised the project. All authors contributed to manuscript preparation.

Conflicts of interest

There are no conflicts to declare.

Data availability

The supporting data has been provided as part of the supplementary information (SI). Supplementary information: synthetic procedure, NMR spectra, and further experimental details. See DOI: https://doi.org/10.1039/d5na01038a.

Acknowledgements

GR and ARL are thankful to Ashoka University for the doctoral research fellowship. We are thankful to the CRF & SATHI facility at IIT Delhi, instrument facility at Shiv Nadar University, and USIC Delhi University for their support in material characterization. We are thankful to Dr Jatish Kumar and Arunima C., IISER Tirupati, for their help in the CPL measurements. The authors gratefully acknowledge the financial aid provided by Axis Bank to support this research work.

References

1 D. Asthana, J. Shukla, S. Dana, V. Rani, M. R. Ajayakumar, K. Rawat, K. Mandal, P. Yadav, S. Ghosh and P. Mukhopadhyay, *Chem. Commun.*, 2015, **51**, 15237–15240.
2 D. Ke, C. Zhan, A. D. Q. Li and J. Yao, *Angew. Chem., Int. Ed.*, 2011, **50**, 3715–3719.
3 W. Zhang and C. Gao, *J. Mater. Chem. A*, 2017, **5**, 16059–16104.
4 S.-Y. Qin, S.-S. Xu, R.-X. Zhuo and X.-Z. Zhang, *Langmuir*, 2012, **28**, 2083–2090.
5 J.-D. Ding, W.-J. Jin, Z. Pei and Y. Pei, *Chem. Commun.*, 2020, **56**, 10113–10126.
6 W. Liang, X. He, N. R. Reddy, Y. Bai, L. An and J. Fang, *Langmuir*, 2019, **35**, 9004–9010.
7 S. M. Wagalgave, D. DucLa, R. S. Bhosale, M. A. Kobaisi, L. A. Jones, S. V. Bhosale and S. V. Bhosale, *New J. Chem.*, 2018, **42**, 6785–6793.
8 Z. Wang, X. Xie, A. Hao and P. Xing, *Angew. Chem., Int. Ed.*, 2024, **63**, e202407182.
9 T. Aida, E. W. Meijer and S. I. Stupp, *Science*, 2012, **335**, 813–817.
10 M. Más-Montoya and R. A. J. Janssen, *Adv. Funct. Mater.*, 2017, **27**, 1605779.
11 H. Cheng, R. Liu, R. Zhang, L. Huang and Q. Yuan, *Nanoscale Adv.*, 2023, **5**, 2394–2412.
12 M. Liu, L. Zhang and T. Wang, *Chem. Rev.*, 2015, **115**, 7304–7397.
13 A. Sengupta, G. Roy, A. R. Likhar and D. Asthana, *Nanoscale*, 2023, **15**, 18999–19015.
14 S. De, D. Asthana, C. Thirmal, S. K. Keshri, R. K. Ghosh, G. Hundal, R. Kumar, S. Singh, R. Chatterjee and P. Mukhopadhyay, *Chem. Sci.*, 2023, **14**, 2547–2552.
15 X. Li, Q. Han, X. Li, R. Li, A. Wang, S. Liang, Y. Sang, J. Li, Y. Tian, Y. Yang, Q. Li, S. Bai and J. Li, *Nat. Commun.*, 2025, **16**, 6044.
16 S. V. Bhosale, M. Al Kobaisi, R. W. Jadhav, P. P. Morajkar, L. A. Jones and S. George, *Chem. Soc. Rev.*, 2021, **50**, 9845–9998.
17 N. Sakai, J. Mareda, E. Vauthey and S. Matile, *Chem. Commun.*, 2010, **46**, 4225–4237.
18 S. V. Bhosale, C. H. Jani and S. J. Langford, *Chem. Soc. Rev.*, 2008, **37**, 331–342.
19 V. Tumiatti, A. Milelli, A. Minarini, M. Micco, A. Gasperi Campani, L. Roncuzzi, D. Baiocchi, J. Marinello,

G. Capranico, M. Zini, C. Stefanelli and C. Melchiorre, *J. Med. Chem.*, 2009, **52**, 7873–7877.
20 V. Pirota, S. Iachettini, C. Platella, P. Zizza, G. Fracchioni, S. Di Vito, A. Carachino, F. Battistini, M. Orozco, M. Freccero, A. Biroccio, D. Montesarchio and F. Doria, *Nucleic Acids Res.*, 2025, **53**, gkaf301.
21 A. A. Ahmed, R. Angell, S. Oxenford, J. Worthington, N. Williams, N. Barton, T. G. Fowler, D. E. O'Flynn, M. Sunose, M. McConville, T. Vo, W. D. Wilson, S. A. Karim, J. P. Morton and S. Neidle, *ACS Med. Chem. Lett.*, 2020, **11**, 1634–1644.
22 B. J. Jung, N. J. Tremblay, M.-L. Yeh and H. E. Katz, *Chem. Mater.*, 2011, **23**, 568–582.
23 F. Würthner and M. Stolte, *Chem. Commun.*, 2011, **47**, 5109–5115.
24 M. Sommer, *J. Mater. Chem. C*, 2014, **2**, 3088–3098.
25 F. Doria, A. Oppi, F. Manoli, S. Botti, N. Kandoth, V. Grande, I. Manet and M. Freccero, *Chem. Commun.*, 2015, **51**, 9105–9108.
26 V. K. Gawade, R. W. Jadhav, V. R. Chari, R. V. Hangarge and S. V. Bhosale, *Anal. Methods*, 2023, **15**, 3727–3734.
27 S. Wu, F. Zhong, J. Zhao, S. Guo, W. Yang and T. Fyles, *J. Phys. Chem. A*, 2015, **119**, 4787–4799.
28 F. S. Etheridge, R. Fernando, J. A. Golen, A. L. Rheingold and G. Sauve, *RSC Adv.*, 2015, **5**, 46534–46539.
29 H. F. Higginbotham, P. Pander, R. Rybakiewicz, M. K. Etherington, S. Maniam, M. Zagorska, A. Pron, A. P. Monkman and P. Data, *J. Mater. Chem. C*, 2018, **6**, 8219–8225.
30 L. J. Rozanski, E. Castaldelli, F. L. M. Sam, C. A. Mills, G. Jean-François Demets and S. R. P. Silva, *J. Mater. Chem. C*, 2013, **1**, 3347–3352.
31 K. Sugiyasu, N. Fujita and S. Shinkai, *Angew. Chem., Int. Ed.*, 2004, **43**, 1229–1233.
32 K. Murata, M. Aoki and S. Shinkai, *Chem. Lett.*, 2006, **21**, 739–742.
33 N. Ponnuswamy, G. D. Pantoş, M. M. J. Smulders and J. K. M. Sanders, *J. Am. Chem. Soc.*, 2012, **134**, 566–573.
34 A. Mukherjee and S. Ghosh, *Org. Mater.*, 2021, **3**, 405–416.
35 A. Das and S. Ghosh, *Chem. Commun.*, 2016, **52**, 6860–6872.
36 Y. Hong, J. W. Y. Lam and B. Z. Tang, *Chem. Commun.*, 2009, 4332–4353, DOI: 10.1039/B904665H.
37 X. Fang, H. Ke, L. Li and M.-J. Lin, *Dyes Pigm.*, 2017, **145**, 469–475.
38 P. Choudhury, S. Sarkar and P. K. Das, *Langmuir*, 2018, **34**, 14328–14341.
39 L. Zong, Y. Xie, C. Wang, J.-R. Li, Q. Li and Z. Li, *Chem. Commun.*, 2016, **52**, 11496–11499.
40 D. A. Shejul, S. M. Wagalgave, R. W. Jadhav, M. A. Kobaisi, D. D. La, L. A. Jones, R. S. Bhosale, S. V. Bhosale and S. V. Bhosale, *New J. Chem.*, 2020, **44**, 1615–1623.
41 J. Kumar, T. Nakashima and T. Kawai, *J. Phys. Chem. Lett.*, 2015, **6**, 3445–3452.
42 F. Salerno, J. A. Berrocal, A. T. Haedler, F. Zinna, E. W. Meijer and L. Di Bari, *J. Mater. Chem. C*, 2017, **5**, 3609–3615.
43 A. R. Likhar, A. Cheran, A. Sengupta, C. Dutta, J. Kumar and D. Asthana, *Chem. Commun.*, 2024, **60**, 9022–9025.
44 Y. Gao, L. Wang, X. Ma, R. Jin, C. Kang and L. Gao, *Chem.–Eur. J.*, 2023, **29**, e202202476.
45 A. Eisfeld and J. S. Briggs, *Chem. Phys.*, 2006, **324**, 376–384.
46 A. P. Deshmukh, N. Geue, N. C. Bradbury, T. L. Atallah, C. Chuang, M. Pengshung, J. Cao, E. M. Sletten, D. Neuhauser and J. R. Caram, *Chem. Phys. Rev.*, 2022, **3**, 021401.
47 K. Cai, J. Xie, D. Zhang, W. Shi, Q. Yan and D. Zhao, *J. Am. Chem. Soc.*, 2018, **140**, 5764–5773.
48 C. Kulkarni and S. J. George, *Chem.–Eur. J.*, 2014, **20**, 4537–4541.
49 A. Insuasty, S. Carrara, J. Xuechen, C. R. McNeill, C. Hogan and S. J. Langford, *Chem.–Asian J.*, 2024, **19**, e202400152.
50 S. M. Wagalgave, S. D. Padghan, M. D. Burud, M. A. Kobaisi, D. D. La, R. S. Bhosale, S. V. Bhosale and S. V. Bhosale, *Sci. Rep.*, 2019, **9**, 12825.
51 A. Sarkar, R. Sasmal, A. Das, A. Venugopal, S. S. Agasti and S. J. George, *Angew. Chem., Int. Ed.*, 2021, **60**, 18209–18216.
52 A. Das and S. Ghosh, *Macromolecules*, 2013, **46**, 3939–3949.
53 C. Röger and F. Würthner, *J. Org. Chem.*, 2007, **72**, 8070–8075.
54 S. V. Bhosale, S. V. Bhosale and S. K. Bhargava, *Org. Biomol. Chem.*, 2012, **10**, 6455–6468.
55 Z. Cao, F. Zhu, A. Hao and P. Xing, *J. Phys. Chem. C*, 2020, **124**, 7965–7972.
56 P. Xing, Y. Li, Y. Wang, P.-Z. Li, H. Chen, S. Z. F. Phua and Y. Zhao, *Angew. Chem., Int. Ed.*, 2018, **57**, 7774–7779.
57 J. Zhang, A. Hao and P. Xing, *Nano Lett.*, 2024, **24**, 16191–16199.
58 H. Svobodová, V. Noponen, E. Kolehmainen and E. Sievänen, *RSC Adv.*, 2012, **2**, 4985–5007.
59 K. Yin, N. Feng, N. Godbert, P. Xing and H. Li, *J. Phys. Chem. Lett.*, 2023, **14**, 1088–1095.
60 H. Shao, J. Seifert, N. C. Romano, M. Gao, J. J. Helmus, C. P. Jaroniec, D. A. Modarelli and J. R. Parquette, *Angew. Chem., Int. Ed.*, 2010, **49**, 7688–7691.
61 M. A. Kobaisi, R. S. Bhosale, M. E. El-Khouly, D. D. La, S. D. Padghan, S. V. Bhosale, L. A. Jones, F. Antolasic, S. Fukuzumi and S. V. Bhosale, *Sci. Rep.*, 2017, **7**, 16501.
62 G. E. Dobretsov, T. I. Syrejschikova and N. V. Smolina, *Biophysics*, 2014, **59**, 183–188.
63 M. Pandeeswar, H. Khare, S. Ramakumar and T. Govindaraju, *RSC Adv.*, 2014, **4**, 20154–20163.
64 S. Basak, N. Nandi, S. Paul and A. Banerjee, *ACS Omega*, 2018, **3**, 2174–2182.
65 A. Insuasty, S. Carrara, J. Xuechen, C. R. McNeill, C. Hogan and S. J. Langford, *Chem.–Asian J.*, 2024, **19**, e202400152.
66 S.-W. Shao, P. Puneet, M.-C. Li, T. Ikai, E. Yashima and R.-M. Ho, *ACS Macro Lett.*, 2024, **13**, 734–740.
67 X. Zhang, J. Yin and J. Yoon, *Chem. Rev.*, 2014, **114**, 4918–4959.